**NURETH14-487** 

# LIQUID FILM THICKNESS OF INDIVIDUAL BUBBLES IN A NARROW CHANNEL

**D. Ito<sup>1</sup>, H.-M. Prasser<sup>1</sup> and M. Aritomi<sup>2</sup>**<sup>1</sup> ETH Zürich, Zurich, Switzerland
<sup>2</sup> Tokyo Institute of Technology, Tokyo, Japan

#### **Abstract**

In this study, the electrical conductance method was applied to measure the liquid film thickness between the individual bubbles and the wall in a narrow channel. This method consists of two different conductance measurements. One measures the conductance between electrodes on an inner wall, and the film thickness is estimated. Other measures the conductance between two sensors which are installed on the opposing walls of the channel. This conductance is related to void fraction in the gap. Therefore, two-dimensional distributions of the liquid film thickness and void fraction can be measured simultaneously.

## 1. Introduction

Development of next-generation light water reactor has been ongoing for sustainable energy supply and multiple recycle of Pu. The practical application of high performance and high conversion BWR becomes imperative. For the high conversion BWR [1][2], it is expected that the triangular dense lattice rod bundle with a narrow rod-to-rod distance is adapted to utilize high neutron energy spectrum. As a result of the dense lattice bundle, the ratio of water as the moderator decreases significantly. So the boiling two-phase flow phenomena in the dense lattice bundle differs greatly from that in the square lattice bundle of the current BWRs. Especially, the flow characteristics in the narrow channel should be clarified. Recently, the numerical works have been carried out for two-phase flow structure in the dense lattice rod bundle [3][4]. However, the accurate experimental data is still required for modelling of the flow and for validation of the numerical simulation. In two-phase flow measurement in the small flow field, the spatio-temporal resolution is very important. Although the radiation methods such as neutron radiography [5] and X-ray tomography [6] could measure two-phase flow structure with high accuracy, some limitations and higher cost make these applications difficult. Thus, it has been hoped that a measurement method with high resolution, ease of use and lower cost is developed for two-phase flow measurement in the dense lattice rod bundle.

For that purpose, the authors focused on the electrical conductance method. Wire-mesh sensor [7][8][9] is one of the successful two-phase flow measurement methods using the electrical conductance. The cross-sectional void fraction distributions in the pipes or the rectangular channels can be obtained by using the difference of the conductance between gas and liquid phases. In addition, it has relatively higher sampling rate up to 10 kHz. In order to measure two-phase flow in narrow channels, the principle of wire-mesh sensor has been applied to the narrow rectangular channel [10]. In this method, the electrode wires are installed on the inner wall of the

channel, and the conductance between the walls is acquired. Therefore, the two-dimensional distribution of void fraction in the narrow gap can be measured. On the other hand, Damsohn and Prasser [11] developed a liquid film sensor, which is based on the electrical conductance measurement between neighbouring electrodes on the wall, for the spatial distribution of the liquid film thickness. Liquid film behaviour on the channel wall has been observed by the sensor. Furthermore, they have applied this method to the subchannel flow in the square lattice and have visualized the liquid films on the rod [12]. Thus, the liquid film thickness and void fraction in the narrow channel can be measured simultaneously by combining above two electrical conductance methods. In other words, two liquid film sensors are installed on the opposing walls of the channel and the electrical conductance on the sensor and between two sensors is measured.

In this study, the liquid film thickness between the individual bubble and the wall is estimated by using the liquid film thickness and void fraction distributions measured by the novel measuring method in the narrow channel with a gap of 1.5 mm. The individual bubbles are identified in the void fraction distribution, and the distribution characteristics of the film thickness on the bubbles are investigated. Finally, the relationship between the liquid film thickness and the bubble size are evaluated.

#### 2. Measurement method

## 2.1 Simultaneous measurement of liquid film thickness and void fraction

A liquid film thickness measurement using the liquid film sensor [11] is combined with gaseous phase detection between electrodes on the opposing walls. For this purpose, a pair of liquid film sensors is installed on both walls of the narrow channel. A schematic diagram of the measurements is given in Figure 1. As long as the conducting liquid phase bridges the narrow gap between the opposing walls, the electrical excitation of a transmitter electrode of one of the film sensors results in the registration of a current at the close-by receiver electrodes of both opposing sensors, while in case of the presence of a bubble, the current to the opposing sensor is interrupted. In the latter case, there is still a current measured at the excited sensor itself, which originates from the conductance of the remaining liquid film covering transmitter and receiver electrodes on this sensor. Hence, the film sensor, at which the transmitter electrodes are activated, can be used to measure the liquid film thickness between the wall and the passing-by bubbles, while the void fraction in the narrow gap is calculated from the conductivity distribution received by the opposing sensor. Repeating the measuring cycle for all transmitter lines, two-dimensional distributions of liquid film thickness and void fraction can be obtained.

In this study, two liquid film sensors (LFS1 and LFS2) are utilized. The electrical conductance measurements are carried out by a wire-mesh electronics unit with 128 transmitter outputs and 128 receiver inputs, from which 16 transmitters and 128 receivers are used. In particular, 16 outputs of the electronics are connected to the transmitter electrodes of the first sensor, LFS1, the 64 receiver electrodes of which occupy the first half of the available inputs of the electronics. In the same time, the receiver electrodes of the LFS2 opposing the LFS1 are connected to the second set of 64 inputs. The transmitter electrodes of the LFS2 are not used and put on ground potential. In this configuration, the maximum measuring frequency can be set to 10 kHz.

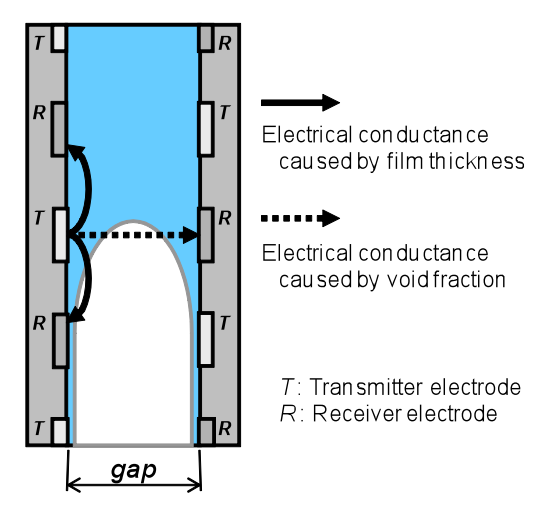


Figure 1 Principle of simultaneous measurement of liquid film thickness and void fraction.

# 2.2 Liquid film sensor

The liquid film thickness on the sensing surface is measured from the conductance between transmitter and receiver electrode lying next to each other. Figure 2 shows the simplified scheme of electrical circuit in the liquid film sensor. Switching the circuit of transmitting side at high speed, the electrical signals are acquired in the receiving circuit. The measured electrical conductance depends on the thickness of the liquid film covering the transmitter and receiver electrode pair.

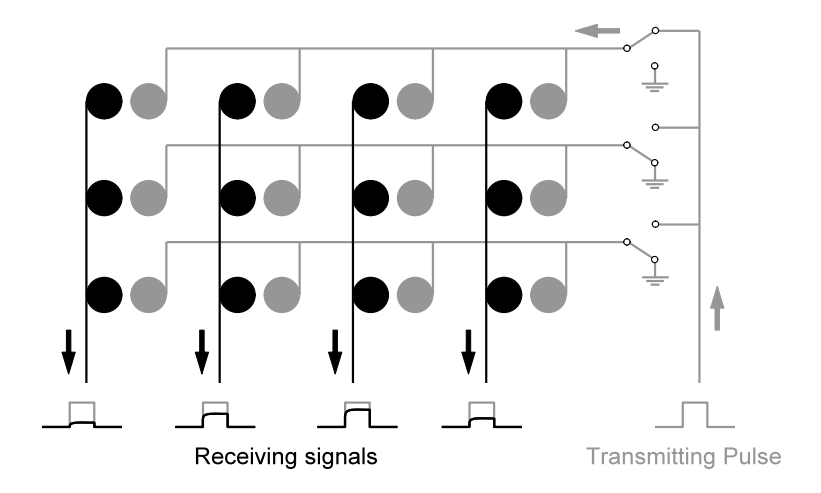


Figure 2 Simplified electrical scheme of liquid film sensor.

The photograph and electrode arrangement of the film sensor are shown in Figure 3. The sensor consists of transmitter, receiver and ground electrodes, and these electrodes are densely arranged, as shown in Figure 3 (a). The distance between measuring electrodes and ground spots is 1 mm. Both transmitter and receiver electrodes have a diameter of 0.5 mm and the ground spots have a diameter of 0.9 mm. The total elementary cell of electrodes has the lateral dimensions of 2 mm,

which is equivalent to the spatial resolution of the measuring matrix, i.e. each measuring point corresponds to a surface area of  $2\times2$  mm<sup>2</sup>.

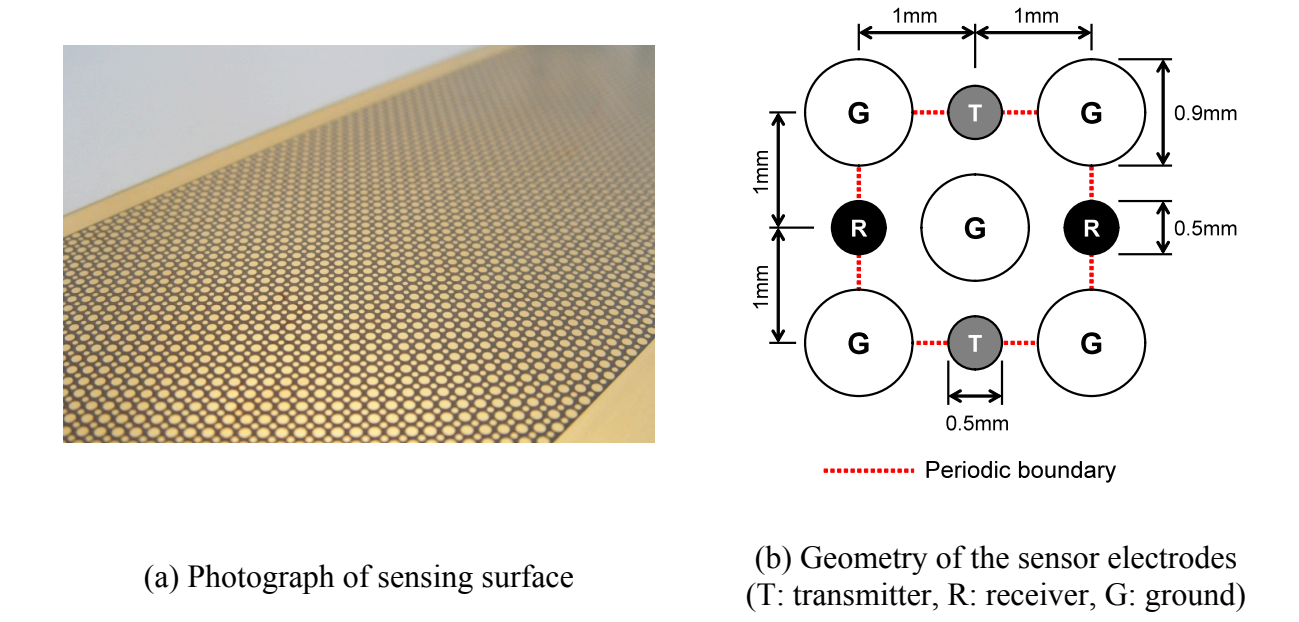


Figure 3 Liquid film sensor used in this study.

# 2.3 Liquid film thickness

In order to estimate the liquid film thickness from measured electrical conductance, the liquid film sensor has to be calibrated. The dependency of the conductance as function of film thickness is non-linear. Furthermore, the instrument constant can vary between individual measuring points due to manufacturing tolerances. In this study, nonconductive cylindrical rollers with the grooves ranging from 100 to 1000  $\mu m$  are applied for the calibration. They are rolled over the sensor which is set in the water. The final signal from the electronic unit is recoded when the roller passes above the electrodes. In this way, the sensor is calibrated together with the signal acquisition electronics. Dimensionless currents are calculated from the ratio of the value measured for a certain known film thickness and the saturation value. The latter is obtained from a measurement with a thickness of the water layer bigger than the sensibility range of the sensor, i.e. a thickness, at which the measured signal converges to the asymptotic one for an infinite water layer.

The calibration results are plotted in Figure 4. The horizontal axis is the dimensionless current and the vertical one is film thickness. These points are the values averaged over the entire measurement points and the standard deviation is represented by the error bar. It is found that the conductance is almost saturated above a thickness of  $600 \, \mu m$ . Hence, the applied film sensor can measure the thickness less than about  $500 \, \mu m$ .

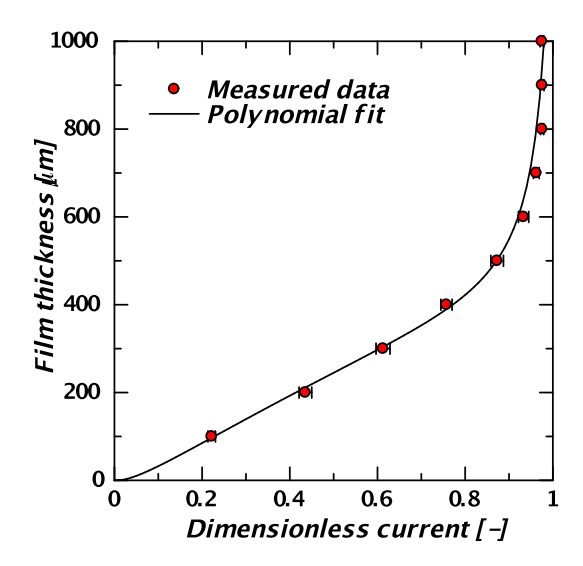


Figure 4 Calibration curve for the film thickness.

A polynomial calibration function based on a fourth-order polynomial is adapted to obtain the film thickness from measured conductance. The denominator of the function is a second order polynomial serving to reflect the asymptotic behaviour of the measuring signal. The coefficients of the function are fitted to match the calibration values. So the film thickness is estimated by the following polynomial equation,

$$\delta = \frac{a_1 x^4 + a_2 x^3 + a_3 x^2 + a_4 x + a_5}{(x - b_1)(x - b_2)} \tag{1}$$

where x is a ratio of measured conductance to saturated one  $(x=\sigma/\sigma_L)$ . In Eq.(1),  $b_1$  and  $b_2$  are the poles of the calibration function. The coefficients  $a_1$  to  $a_5$  are estimated individually for each measurement point in the two-dimensional sensor matrix. The result of the polynomial fit is also shown as a solid line in Figure 4. This curve reflects well the measured results.

### 2.4 Void fraction

The local void fraction between transmitter and receiver electrodes opposing each other can be calculated from the measured conductance. This principle is the same as wire-mesh sensors. In the liquid film sensor used in this study, there are a lot of ground electrodes, so electrical field between two sensors has high directive property. This implies that the local conductance signal originates from a small focus area around the center of mass of the active electrodes. In this study, the void fraction is assumed to be proportional to the electrical conductance. Thus the following equation is used to estimate the instantaneous local void fraction from measured conductance in the narrow gap.

$$\varepsilon = 1 - \frac{\sigma}{\sigma_I} \tag{2}$$

where  $\sigma$  is the measured electrical conductance and  $\sigma_L$  is the conductance of plain liquid.

To evaluate the individual bubble parameters, the bubble identification is performed in the void fraction array by using recursive fill algorithm, which has been used in the previous studies using wire-mesh sensor [9]. Bubble is recognized as a mass of points with higher void fractions in the measured distribution. From the void fraction data, the individual bubbles are indentified by connecting the points with the void fraction above a threshold and a unique bubble identifier n is given for each point. Then, the bubble volume for an identified bubble is estimated by integrating the local void fractions over the elements of the void fraction array with the same bubble identifier, as follows,

$$V_b = s\Delta x \Delta y \sum_{i,j} \varepsilon \tag{3}$$

where  $\Delta x$  and  $\Delta y$  are the distance between measurement points, *i* and *j* are the indices of *x* and *y* direction, respectively. The volume equivalent diameter of the bubble is calculated as

$$D_{eq} = \sqrt[3]{\frac{6}{\pi}V_b} \ . \tag{4}$$

In addition, the bubble length  $L_b$  in the flow direction is also estimated from the distance between the front and back ends of the identified bubble.

## 3. Experimental set-up

The schematic diagram of the test channel is illustrated in Figure 5. The narrow rectangular channel with a width of 32 mm and a gap distance of 1.5 mm is used. So the aspect ratio of the channel cross section is 21.3 and the equivalent hydraulic diameter is 2.87 mm. The length of the test channel is 1450 mm and the width is constant over height. The flow is a vertical upward airwater flow at room temperature under atmospheric condition. Water is supplied from the lower part of the channel, and the flow rate is monitored by a rotameter. Air is injected from an orifice with 0.5 mm diameter in the front wall at a height of 170 mm from the water inlet and a center point of channel width. The air flow rate is controlled by a mass flow controller (MFC). The airwater mixture passes through the test section and exits from the upper part of the channel. The measurement section is located at a height of 900 mm from the air inlet.

The superficial velocities of the gas and liquid phases are used to represent the flow condition and they are calculated from each flow rate and the cross-sectional area. In order to evaluate the individual bubbles, bubbly and slug flows are formed in the test section by varying the superficial liquid and gas velocities.

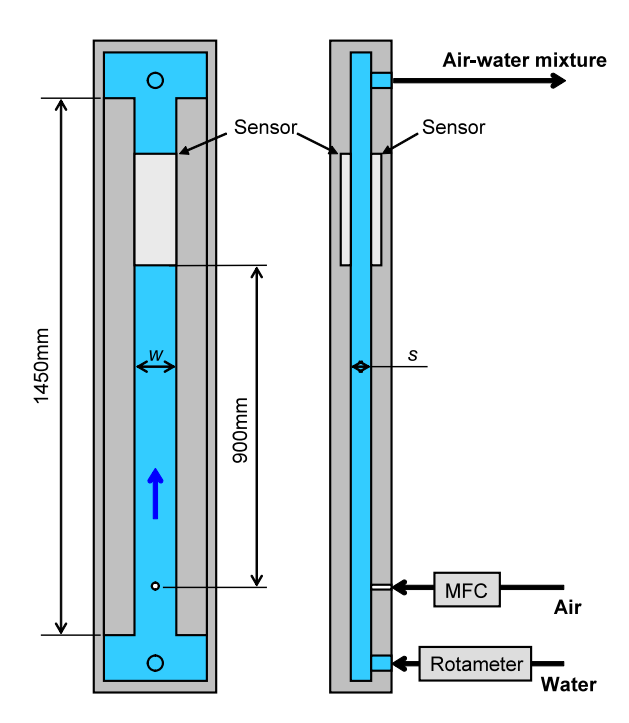


Figure 5 Schematic diagram of test channel.

A pair of film sensors is installed on both front and back walls of the channel. Both sensors together form a measuring matrix of 16 transmitters and 128 receivers with a total number of 2048 measurement points. At this size of the sensor matrix, the applied wire-mesh sensor electronics unit allows to run the measurement at a speed of 10 kHz. In the result,  $16\times64$  (=1024) points are available for the measurement of the liquid film thickness, and other  $16\times64$  (=1024) points are used for the void fraction measurement. The spatial resolution of both sensors is  $2\times2$  mm<sup>2</sup>. Therefore, the instrumented area has the dimensions of  $32\times128$  mm<sup>2</sup>.

### 4. Results and discussion

# 4.1 Distribution characteristics of liquid film thickness

The typical instantaneous distributions of liquid film thickness between bubbles and the channel wall are shown in Figure 6 and Figure 7. The bubbles are plotted by the void fraction with a color map (white:  $\varepsilon = 100$  %, blue:  $\varepsilon = 0$  %), and the value of the liquid film thickness is represented by contour lines. The unit of the labels for the liquid film thickness in the distribution is micro meter ( $\mu$ m). Figure 6 shows the results of bubbles with the size of  $D_{eq} = 15\sim16$  mm and Figure 7 shows the results of larger bubbles with  $D_{eq} = 19\sim20$  mm. The size of bubbles is changed by controlling the superficial gas velocity. It is found that the film thickness in the middle part of bubbles is thin. The liquid film is entrained by the bubble motion and this is due to the surface tension in the meniscus formed by the confined narrow channel. This can be seen not only for small bubbles but also for large bubbles. Furthermore, the thickness increases with a growth of superficial liquid velocity, however, the bubble has thin liquid film ( $\sim10~\mu$ m) at the both ends even for high velocity condition.

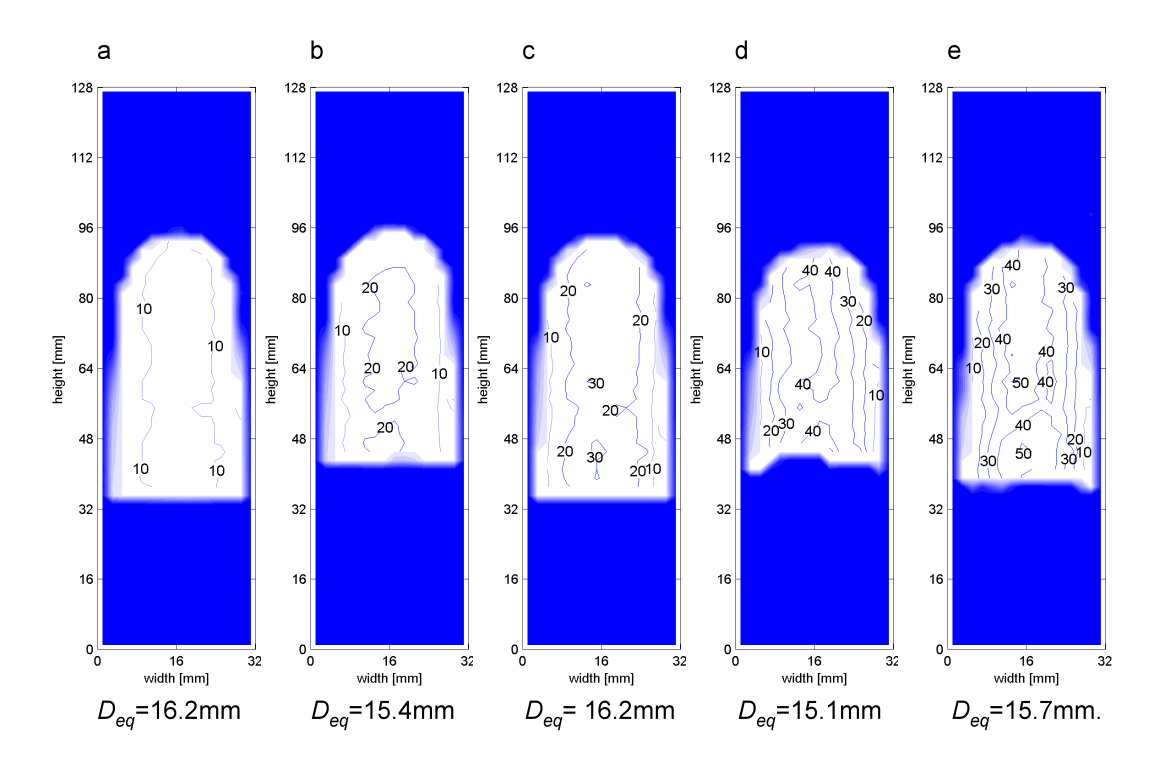


Figure 6 Instantaneous distributions of film thickness in individual bubbles, (a)  $J_L$ =0.029m/s, (b)  $J_L$ =0.087m/s, (c)  $J_L$ =0.17m/s, (d)  $J_L$ =0.26m/s, (e)  $J_L$ =0.35m/s.

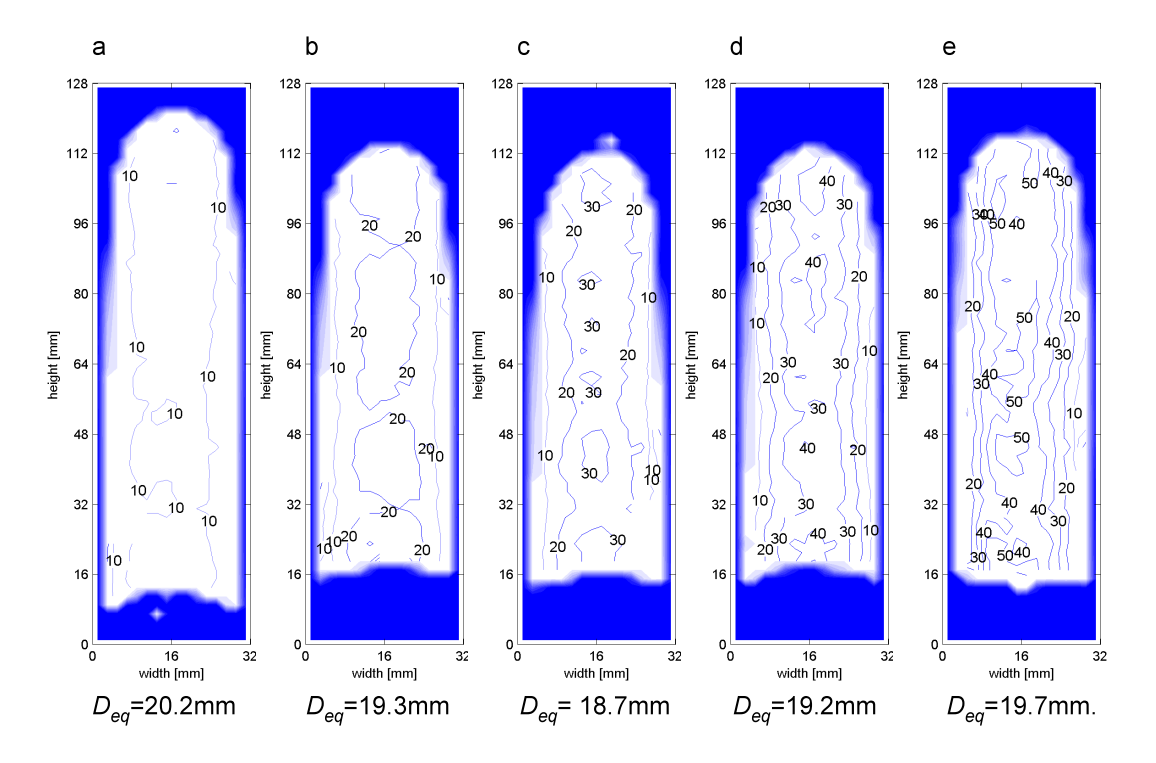


Figure 7 Instantaneous distributions of film thickness in individual large bubbles, (a)  $J_L$ =0.029m/s, (b)  $J_L$ =0.087m/s, (c)  $J_L$ =0.17m/s, (d)  $J_L$ =0.26m/s, (e)  $J_L$ =0.35m/s.

In the previous studies on two-phase flow in the narrow rectangular channel, two-dimensional projected information has been used to evaluate the flow structure. However, from these results, it is found that liquid film occupies about 7 % of the channel gap at high liquid velocity. Therefore, the liquid film thickness between bubble and the wall has to be considered for high accurate bubble estimation in the narrow channel.

## 4.2 Liquid film thickness for individual bubbles

The thickness of the individual bubbles is calculated by using the bubble identification algorithm. The bubble size and mean film thickness on the bubble are estimated for a lot of different individual bubbles placed within the measurement area. Figure 8 shows the individual bubble characteristics. The bubble diameter and length for each bubble is plotted in Figure 8(a). There is a relation between bubble diameter and length. However, the variation of plots increases when superficial liquid velocity increases, because the shape of bubbles is rather changed by the liquid flow. The maximum measurable bubble size depends on the volume of the sensing section of the sensor  $(32\times128\times1.5 \text{ mm}^3)$ , and so  $D_{eq,max} = 22.7 \text{ mm}$  and  $L_{b,ma}$  = 128 mm in this measurement. The liquid film thickness on the bubble is averaged over the bubble and plotted in Figure 8(b). The averaged film thickness decreases as equivalent bubble diameter increases. Furthermore, it is found that the film thickness becomes larger as increasing superficial liquid velocity, as mentioned above.

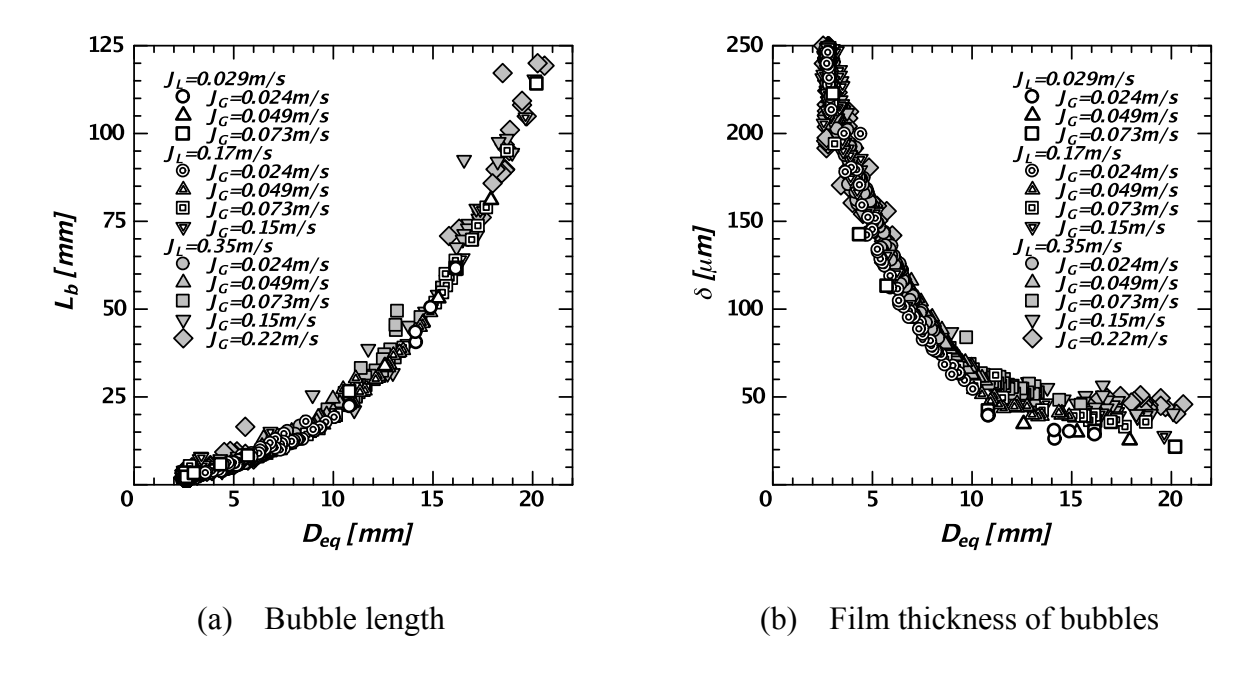


Figure 8 Individual bubble parameters.

Figure 9 shows the mean liquid film thicknesses between the bubbles and the wall at each superficial liquid velocity. The liquid film thickness is averaged for the individual bubbles with the equivalent diameter more than 10 mm because the number of small bubbles is many and the difference of film thickness is less. In this graph, it is clear that the mean film thickness on the

bubble increases with superficial liquid velocity. This is explained by growth of the liquid flow in between bubbles and the wall.

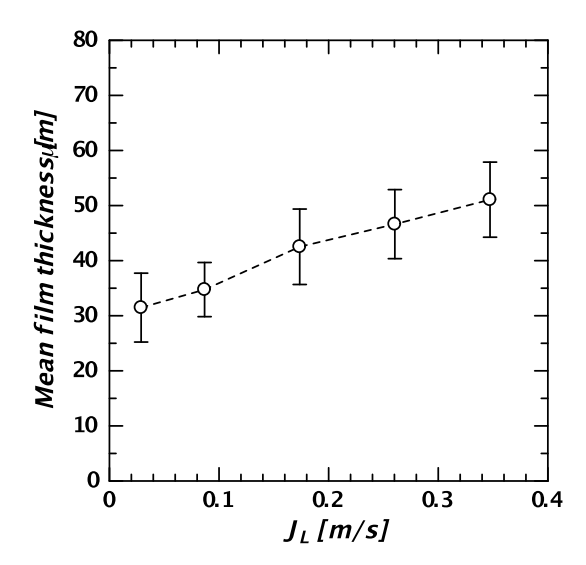


Figure 9 Mean film thickness for the bubbles with  $D_{eq} > 10$  mm.

#### 5. Conclusions

Liquid film behaviour on the individual bubbles in a narrow rectangular channel with a gap of 1.5 mm was studied by using liquid film sensors which are based on electrical conductance method. The liquid film thickness distributions between bubbles and the wall were determined on a two-dimensional domain. The arrangement of sensors on both front and back walls of the test channel allowed measuring film thickness and void fraction simultaneously. In the void fraction distribution, the individual bubble was identified and the corresponding film thickness between the bubble and the wall was estimated in the film thickness distribution. The liquid films were not distributed uniformly on the bubble and the dimple of liquid film was found in the middle part of bubbles. The depth of the dimple increases with increasing of superficial liquid velocity.

#### 6. References

- [1] T. Iwamura et al., "Concept of innovative water reactor for flexible fuel cycle (FLWR)", Nuclear Engineering and Design, Vol. 236, 2006, pp.1599-1605.
- [2] S. Uchikawa et al., "Conceptual design of innovative water reactor for flexible fuel cycle (FLWR) and its recycle characteristics", Journal of Nuclear Science and Technology, Vol. 44, No. 3, 2007, pp.277-284.
- [3] W. Zhang et al., "Numerical investigation of cross flow phenomena in a tight-lattice rod bundle using advanced interface tracking method", Journal of Power Energy and Systems, Vol. 2, No. 2, 2008, pp. 465-466.

- [4] H. Yoshida et al., "Numerical simulation of boiling two-phase flow in tight-lattice rod bundle by 3-dimensional two-fluid model code ACE-3D", Journal of Power Energy and Systems, Vol. 3, No. 1, 2009, pp. 204-215.
- [5] M. Kureta, "Experimental study of three-dimensional void fraction distribution in heated tight-lattice rod bundles using three-dimensional neutron tomography", Journal of Power Energy and Systems, Vol. 1, No. 3, 2007, pp. 225-238.
- [6] H.-M. Prasser et al., "Comparison between wire-mesh sensor and ultra-fast X-ray tomograph for an air-water flow in a vertical pipe", Flow Measurement and Instrumentation, Vol.16, No.2-3, 2005, pp. 73-83.
- [7] H.-M. Prasser et al., "A new electrode-mesh tomograph for gas-liquid flows", Flow Measurement and Instrumentation, Vol.9, No.2, 1998, pp. 111-119.
- [8] S. Richter et al., "Approach towards spatial phase reconstruction in transient bubbly flow using a wire-mesh sensor", International Journal of Heat and Mass Transfer, Vol.45, No.5, 2002, pp. 1063-1075.
- [9] D. Ito et al., "Uncertainty and intrusiveness of three-layer wire-mesh sensor", Flow Measurement and Instrumentation, Vol. 22, 2011, pp.249-256.
- [10] D. Ito et al., "Micro wire-mesh sensor for two-phase flow measurement in a narrow rectangular channel", Flow Measurement and Instrumentation, 2011, In Press, doi:10.1016/j.flowmeasinst.2011.06.001.
- [11] M. Damsohn and H.-M. Prasser, "High-speed liquid film sensor for two-phase flows with high spatial resolution based on electrical conductance", Flow Measurement and Instrumentation, Vol.20, 2009, pp.1-14.
- [12] M. Damsohn and H.-M. Prasser, "Experimental studies of the effect of functional spacers to annular flow in subchannels of a BWR fuel element", Nuclear Engineering and Design, Vol. 240, No. 10, 2010, pp. 3126-3144.